Liquid Domains in Vesicles Investigated by NMR and Fluorescence Microscopy

S. L. Veatch,* I. V. Polozov,† K. Gawrisch,† and S. L. Keller*
*Departments of Chemistry and Physics, University of Washington, Seattle, Washington; and †Laboratory of Membrane Biochemistry and Biophysics, National Institute on Alcohol Abuse and Alcoholism, National Institutes of Health, Rockville, Maryland

ABSTRACT We use ^{2}H-NMR, ^{1}H-MAS NMR, and fluorescence microscopy to detect immiscibility in three particular phospholipid ratios mixed with 30% cholesterol: 2:1 DOPC/DPPC, 1:1 DOPC/DPPC, and 1:2 DOPC/DPPC. Large-scale ($\gg$160 nm) phase separation into liquid-ordered (L_o) and liquid-crystalline (L_α) phases is observed by both NMR and fluorescence microscopy. By fitting superimposed ^{2}H-NMR spectra, we quantitatively determine that the L_o phase is strongly enriched in DPPC and moderately enriched in cholesterol. Tie-lines estimated at different temperatures and membrane compositions are based on both ^{2}H-NMR observations and a previously published ternary phase diagram. ^{2}H- and ^{1}H-MAS NMR techniques probe significantly smaller length scales than microscopy experiments (submicron versus micron-scalp), and complex behavior is observed near the miscibility transition. Fluorescence microscopy of giant unilamellar vesicles shows micrometer-scale domains below the miscibility transition. In contrast, NMR of multilamellar vesicles gives evidence for smaller ($\sim$80 nm) domains just below the miscibility transition, whereas large-scale demixing occurs at a lower temperature, T_{low}. A transition at T_{low} is also evident in fluorescence microscopy measurements of the surface area fraction of ordered phase in giant unilamellar vesicles. Our results reemphasize the complex phase behavior of cholesterol-containing membranes and provide a framework for interpreting ^{2}H-NMR experiments in similar membranes.

INTRODUCTION

There is mounting evidence that the plasma membrane of many cells is inhomogeneous. Raft domains in cell membranes are thought to preferentially contain cholesterol and saturated lipids, as well as specific lipids (e.g., sphingomyelin and the ganglioside GM1) and proteins (e.g., certain receptors and proteins with palmitoyl or glycosylphosphatidylinositol anchors) (Brown and London, 1998; Simons and Ikonen, 1997). The list of important physiological processes in which rafts are thought to play a role is long (see McIntosh et al., 2003, and references therein).

Recently, several research groups have used giant unilamellar vesicles (GUVs) as models of cell plasma membranes (Baumgart et al., 2003; Dietrich et al., 2001; Samsonov et al., 2001). Using fluorescence microscopy, two of us (S.L.V. and S.L.K.) have observed coexisting liquid phases in GUVs containing ternary mixtures of cholesterol, saturated lipids, and unsaturated lipids (Veatch and Keller, 2002, 2003a,b). The domains disappear into one uniform liquid phase when temperature rises above the miscibility transition.

In our previous work, we studied the ternary mixture of DOPC, DPPC, and cholesterol in depth. We presented qualitative conclusions that one of the liquid phases is rich in cholesterol and saturated lipids, and the other in unsaturated lipids (Veatch and Keller, 2003b). The primary goal of our current work is to quantify the amount of each lipid in the two liquid phases as a function of both temperature and composition. To accomplish this, we employ nuclear magnetic resonance (NMR) on multilamellar vesicles (MLVs). NMR has been used previously by one of us (K.G.) to evaluate lateral lipid organization and the cholesterol-induced increase in phospholipid chain order (Huster and Arnold, 1998).

We argue that it is increasingly important to study the same membrane system by a variety of methods. This is particularly pertinent because each method has different experimental advantages, and can lead to different conclusions about the size of domains and the temperature of the miscibility transition (Anderson and Jacobson, 2002; Silvius, 2003). Along these lines, NMR has been recently utilized to search for inhomogeneities in the same lipid membranes used in microscopy experiments (Aussenac et al., 2003; van Duyl et al., 2003). Other than fluorescence microscopy and NMR, a wealth of other techniques have been employed to study lipid organization of model and cellular membrane systems, including electron spin resonance, fluorescence resonance energy transfer, fluorescence recovery after photobleaching, differential scanning calorimetry, fluorescence anisotropy, freeze-fracture electron microscopy, and extraction of detergent-resistant domains (Alecio et al., 1982; Gidwani et al., 2001; Kenworthy et al., 2000; Lentz et al., 1980; London and Brown, 2000; McMullen and McElhaney, 1995; Shimshick and McConnell, 1973).

In this article, we report observations of liquid immiscibility in model membranes by NMR and fluorescence

Submitted October 6, 2003, and accepted for publication December 5, 2003.

Address reprint requests to Sarah L. Keller, University of Washington, Dept. of Chemistry, Seattle, WA 98195-1700. Tel.: 206-543-9613; E-mail: slkeller@chem.washington.edu.

Abbreviations used: GUV, giant unilamellar vesicle; MLV, multilamellar vesicle; ^{2}H-NMR, deuterium NMR; ^{1}H-MAS NMR, proton magic angle spinning NMR; L_α, liquid crystalline; L_o, liquid ordered; DOPC, 1,2-dioleoyl-*sn*-glycero-3-phosphocholine; DPPC, 1,2-dipalmitoyl-*sn*-glycero-3-phospocholine; Chol, cholesterol; Chol-d1, cholesterol deuterated at the 3α carbon; DPPC-d62, 1,2-dipalmitoyl-d62-*sn*-glycero-3-phosphocholine.

0006-3495/04/05/2910/13 $2.00

microscopy. We verify the existence of a liquid-ordered phase, quantify the lipid composition of coexisting phases, and estimate tie-lines in the DOPC/DPPC/Chol miscibility phase diagram. In addition, we observe complex behavior by ^{2}H-NMR near the miscibility transition temperature and compare it to results from parallel fluorescence microscopy experiments. To our knowledge, this is the first report combining these two experimental methods to study liquid demixing in bilayer membranes, and we believe that our results are relevant to recent ^{2}H-NMR experiments in similar membrane systems.

MATERIALS AND METHODS

Commercial reagents

1,2-Dioleoyl-*sn*-glycero-3-phosphocholine (DOPC), 1,2-dipalmitoyl-*sn*-glycero-3-phospocholine (DPPC), cholesterol (Chol), and 1,2-dipalmitoyl-d62-*sn*-glycero-3-phosphocholine (DPPC-d62) were obtained from Avanti Polar Lipids (Alabaster, AL). Cholesterol deuterated at the 3α position (Chol-d1) was obtained from Cambridge Isotope Laboratories (Andover, MA). All lipids were used without further purification and were stored in chloroform at −20°C until use. Texas Red 1,2-dipalmitoyl-*sn*-glycero-3-phosphoethanolamine (TR-DPPE, Molecular Probes, Eugene, OR) was used as a dye for contrast between phases in fluorescence experiments.

Sample preparation

MLVs

For ^{2}H-NMR experiments, each sample contained 10 mg of deuterated lipid. For ^{1}H-MAS NMR experiments, 5 mg total lipid was prepared. Lipids were mixed in chloroform and then dried under argon while rotating to form a thin film. Samples were exposed to vacuum (<10 mm Hg) for at least 30 min to remove any remaining solvent. Lipids were hydrated at 50 w/w with deuterium-depleted H_2O (^{2}H-NMR) or D_2O (^{1}H-MAS NMR) to form multilamellar vesicles and spun into NMR tubes. Samples were stored at −80°C until use.

GUVs

Giant unilamellar vesicles (GUVs) were prepared using electroformation (Angelova et al., 1992) as described in Veatch and Keller (2003b). Vesicles were prepared in >18 MΩ/cm water and grown for 1 h at 60 ± 3°C. The growth temperature was chosen to be the maximum that consistently produced high yields of GUVs. Vesicles were stored warm for at most 2 h before observation. Although deposited lipids were uniformly mixed, the resulting vesicles varied slightly in composition, estimated at <2 mol %. Significantly longer growth times and lower growth temperatures resulted in altered composition of all vesicles in a sample. Composition differences were observed in vesicles as different miscibility transition temperatures, surface fraction of dark phase, or brightness (mol % dye).

^{2}H-NMR

Instrument settings

^{2}H-NMR powder spectra were acquired on a Bruker DMX300 (Bruker BioSpin Corp., Billerica, MA) spectrometer at a resonance frequency of 46.1 MHz using a stationary dual resonance probe with a 4-mm solenoidal sample coil. Sample temperature was controlled to ±0.1°C by a Bruker variable temperature control unit. Absolute sample temperature was calibrated to within ±0.5°C. A quadrupolar echo sequence (Davis et al., 1976) was used with two 1.8-μs 90° pulses and an interpulse delay of 50 μs. For all experiments, the carrier frequency of the instrument was placed at the center of the spectrum. Typically 7200 scans (DPPC-d62) or 100,000 scans (Chol-d1) with a spectral width of 200 kHz and a delay time of 0.2 s were acquired. To accurately determine DPPC-d62 distribution between coexisting phases for samples of 1:2 DOPC/DPPC-d62 + 30% cholesterol, the delay time between acquisitions was increased to 2 s. Before Fourier transformation, the resonances, detected in quadrature detection mode, were phase-corrected to minimize intensity in the imaginary channel. The echo maximum in the real channel was determined with a resolution of 1/10th of a dwell (DW) time unit. A time-base-corrected free induction decay (FID) was calculated by spline interpolation between data points to begin exactly at the echo maximum. An exponential line-broadening of 100 Hz for DPPC-d62 and 300 Hz for Chol-d1 membranes was applied to the free induction decay before performing the Fourier transformation.

Spectra fitting

Effective quadrupole coupling constants $\Delta\nu_x$ were determined by dePakeing of the Fourier transformed spectra (McCabe and Wassall, 1995; Sternin et al., 1983). For spectral simulations the FID of spectra, $y_{x,n}$, were calculated according to the equation

$$y_{x,n} = \sum_{n1} \cos(2\pi\Delta\nu_x \times S(\theta_{n1}) \times n \times DW) \times \sin(\theta_{n1}) \times \Delta\theta_{n1},$$

where the order parameter is $S(\theta_{n1}) = \frac{1}{2}(3\cos(\theta_{n1}) - 1)$ and θ_{n1} is the angle between the magnetic field and the bilayer normal. The angle θ_{n1} was incremented in 90 $n1$-steps from 0 to $\pi/2$. The dwell time is the time increment between data points in the FID, and n is the number of data points per FID (typically 4096). Spectra for the different $\Delta\nu_x$-values were calculated separately and then superimposed. Intensities and line-broadening were determined by fitting to an experimental lineshape utilizing a Marquardt-Levenberg least-squares algorithm through the *lsqnonlin* routine in Matlab 5 (Mathworks, Natick, MA). Errors in signal intensity were determined directly from the covariance matrix at the solution and correlation coefficients between linewidth and intensity varied between 0.4 and 0.6. A systematic error in relative signal intensity is present in data from 1:1 and 2:1 DOPC/DPPC-d62 + 30% cholesterol membranes due to short delay times between data acquisitions. This data was corrected by increasing the relative intensity of the disordered phase by 15% ± 10%. This scale factor was determined from the difference in disordered phase signal intensities spectra with delay times of 0.2 s and 2 s between acquisitions in membranes of 1:2 DOPC/DPPC-d62 + 30% cholesterol. The intensity ratio of the superimposed Chol-d1 spectra was determined by fitting Gaussian lines to the dePaked spectra using the Marquardt-Levenberg algorithm as described above.

Domain size

The appearance of ^{2}H-NMR spectra for regions of phase coexistence provides a means for obtaining upper and lower bounds of domain size. The calculation assumes that lipids perform lateral diffusion at a rate of $D = 1 \times 10^{-11}$ m^{2}s^{-1} (Gaede and Gawrisch, 2003) that is unimpeded by phase boundaries. Because of differences in lipid composition of domains, particularly in cholesterol content, the chain order parameters of DPPC-d62 differ in liquid-ordered and liquid-crystalline environments. For simplicity we assumed that appearance of powder spectra is dominated by resonances from bilayers oriented with their normal perpendicular to the magnetic field, the most intense resonances in the spectrum. Exchange of lipids between domains at a rate of $k \ll \pi\Delta\nu_q$, where $\Delta\nu_q$ is the difference in quadrupole splittings between domains, results in a superposition of spectra from both domains. If $k \approx \pi\Delta\nu_q$, then spectra are broad and unresolved, and if $k \gg$

$\pi\Delta\nu_q$, then the quadrupole splitting is the well-resolved arithmetic average of splittings in the domains. If we assume for simplicity that the size of liquid-ordered and liquid-crystalline domains is the same, then the lifetime of lipids in those domains is $\tau_o = \tau_d = 2/k$ and the domain diameter is $d_o = 2\sqrt{4D\tau_o}$.

M1 determination

The first moment of a ^{2}H-NMR spectrum is defined to be $M1 = \frac{1}{A}\sum_i |\omega_i I_i|$ where $A = \sum_i I_i$, the total area under the spectrum, and I_i is the intensity of the ^{2}H-NMR spectra at frequency ω_i. The origin of the frequency axis was defined as the center of symmetry of the spectra. The limits for the $M1$ integration were chosen to be symmetric around the origin and completely enclose the observed spectra.

Cholesterol wobble

Cholesterol wobble angles were calculated as described in Brzustowicz et al. (2002) and Oldfield et al. (1978) and summarized here. It is assumed that the 3α C-^{2}H bond of cholesterol adopts an angle of 79° to the bilayer normal, corresponding to an order parameter of $S_{orient} = -0.445$ (Taylor et al., 1981). The order parameter is further reduced by a wobble of the cholesterol main axis according to $S_{effective} = S_{wobble}\, S_{orient}$. The wobble angle θ_0 was determined by numerical integration assuming that θ obeys an axially symmetric Gaussian distribution:

$$S(\theta_0)_{wobble} = \frac{1/2\sum_{n1}(3\cos^2\theta_{n1} - 1)\exp(\theta_{n1}^2/2\theta_o^2)\sin(\theta_{n1})\Delta\theta_{n1}}{\sum_{n1}\exp(\theta_{n1}^2/2\theta_o^2)\sin(\theta_{n1})\Delta\theta_{n1}}.$$

^{1}H-MAS NMR

NMR experiments with magic angle spinning (MAS) were conducted on a Bruker DMX500 widebore spectrometer at a resonance frequency of 500.13 MHz and a spectral width of 50 kHz. Sample spinning at 10 kHz was accomplished in a Bruker double-gas-bearing MAS probe head for 4 mm rotors. Samples were loaded into an 11 μL spherical MAS rotor insert. ^{1}H-NMR spectra were acquired in quadrature detection mode with a delay time between acquisitions $d_1 = 10$ s. For temperature control the MAS bearing air was passed through a copper coil immersed in a cooling bath and then reheated by a Bruker VT control unit. The temperature inside the spinning rotor was calibrated by measuring the chemical shift difference between water and choline in a micellar sample of 1,2-dicaproyl-*sn*-glycero-3-phosphocholine (Avanti Polar Lipids, Alabaster, AL). The chemical shift as a function of temperature was measured on the same sample in a 5 mm tube in a high resolution probe whose temperature had been calibrated precisely with a thermocouple. Spectra were recorded at 2°C intervals over the temperature range from 8 to 45°C. Results were analyzed by plotting peak height as a function of temperature. The weak temperature dependence of peak width in the fluid L_α phase was suppressed by multiplication of the free induction decay with an exponential function before Fourier transformation, equivalent to a line-broadening of 100 Hz.

Fluorescence

Miscibility transition temperatures

GUV samples were viewed as described in Veatch and Keller (2003b). Miscibility transition temperatures (T_{mix}) were determined by first ramping to a temperature near the transition (0.2°C/s) and then allowing the stage and sample to equilibrate for ~60 s before observation. This provides ample time for the stage to equilibrate and the thermistor to respond. This process was repeated in increments of ~0.5°C. Varying TR-DPPE from 0.2 to 2 mol % in vesicles of 1:1 DOPC/DPPC + 30% cholesterol produced a scatter in miscibility transition temperatures of <1°C, which is on the order of the experimental error and demonstrates that the concentration of TR-DPPE is not crucial.

Surface fraction of phases

Immediately after preparation, GUVs were quenched from 60°C by transfer onto a precooled stage. Images of the top and bottom hemispheres of vesicles were collected for a minimum of 10 vesicles at each quench temperature. The brightness of each phase varied across the vesicle due to both vesicle geometry and scatter from probes located outside the focal volume. These difficulties made it impossible to calculate the surface fraction of phases by simple automated algorithms, so boundaries between bright and dark phases were determined by hand. To determine the errors introduced by hand processing, all images were analyzed by two investigators. Trends in surface fraction versus temperature were independent of the investigator, although absolute surface fractions differed by up to 20%. The surface fraction of the dark phase was determined by first averaging the top and bottom faces of each vesicle, and then averaging over all vesicles. Due to the limited depth of focus of our objective, statistical errors are primarily due to capturing less than the full vesicle hemisphere, particularly when domains were large and nonuniformly distributed. To reduce statistical errors, vesicles were preferentially viewed shortly after phase separation, when domains are smaller and more uniformly distributed across the membrane. We observe the same average surface fraction of dark phase independent of domain size (within statistical error), implying that the composition of the phases equilibrates quickly, before domains have ripened to their equilibrium sizes. Near the transition temperature, photo-oxidation likely introduces additional errors (Veatch and Keller, 2003b). Since the surface fraction of phases is sensitive to vesicle growth temperature, time, and storage conditions, extra effort was made to control experimental conditions.

Determination of tie-lines

Tie-lines passing through three points in the ternary phase diagram of DOPC, DPPC, and cholesterol are estimated. First, the fraction of total lipids that were DPPC (or Chol) in each phase was evaluated by multiplying the ^{2}H-NMR partitioning measurements shown below in Fig. 8 by the fraction of DPPC (or Chol) in each membrane preparation. From these values, DPPC/Chol ratios were determined for the L_o and L_α phases. DPPC-d62 partitioning data is offset by $+2.5 \pm 1$°C to account for the depressed transition temperature in membranes containing deuterated DPPC. Second, lines are drawn along the DPPC/Chol ratios for the L_o and L_α phases, with suitable composition errors. Third, the lines for the DPPC/Chol ratios intersect the appropriate miscibility phase boundary at a range of physical solutions for the coexisting L_o and L_α phase compositions. Since our ^{2}H-NMR data gives phase compositions of only two of the three components (DPPC and cholesterol), it is assumed that miscibility phase boundaries determined by fluorescence microscopy are applicable (Veatch and Keller, 2003b). Termini are constrained to be those points connected by a tie-line that passes through the overall vesicle composition.

RESULTS AND DISCUSSION

In previous work, we used fluorescence microscopy to study vesicles containing DOPC, DPPC, and cholesterol over a wide composition and temperature range (Veatch and Keller, 2003b). We found that the ternary phase diagram contained a large region of coexisting liquid phases which

are presumably liquid crystalline (L_α) and liquid ordered (L_o). In the present study, we focus on three particular phospholipid ratios mixed with 30% cholesterol: 2:1 DOPC/DPPC, 1:1 DOPC/DPPC, and 1:2 DOPC/DPPC. Fig. 1 shows these three mixtures in the context of a ternary phase diagram at 25°C (Veatch and Keller, 2003b). The specific compositions were chosen for a number of reasons:

1. All mixtures fall within the liquid coexistence region.
2. At 30% cholesterol, only liquid phases and no solids are expected, down to our lowest temperature of 10°C (McMullen and McElhaney, 1995; Vist and Davis, 1990).
3. The three mixtures produce a range both of miscibility transition temperatures and of surface fractions of dark phase.
4. Cholesterol concentrations of 30% are readily obtained when vesicles are made by a variety of different methods (Huang et al., 1999; Silvius, 2003).

In ^{2}H-NMR experiments, either DPPC was replaced by deuterated DPPC-d62, or cholesterol by Chol-d1. The substitution of deuterated DPPC-d62 lowered the mixture's miscibility transition temperature by a few degrees (Table 1), but had no other effect on vesicles viewed by fluorescence microscopy. We have previously shown that the miscibility transition temperature (T_{mix}) scales with chain-melting temperature for ternary mixtures of saturated PCs, DOPC, and cholesterol (Veatch and Keller, 2003b). This relationship predicts that T_{mix} for membranes containing DPPC-d62 should be depressed by ~2.5°C. This is consistent with our measurements of T_{mix} in 1:1 and 1:2 DOPC/DPPC + 30% cholesterol membranes.

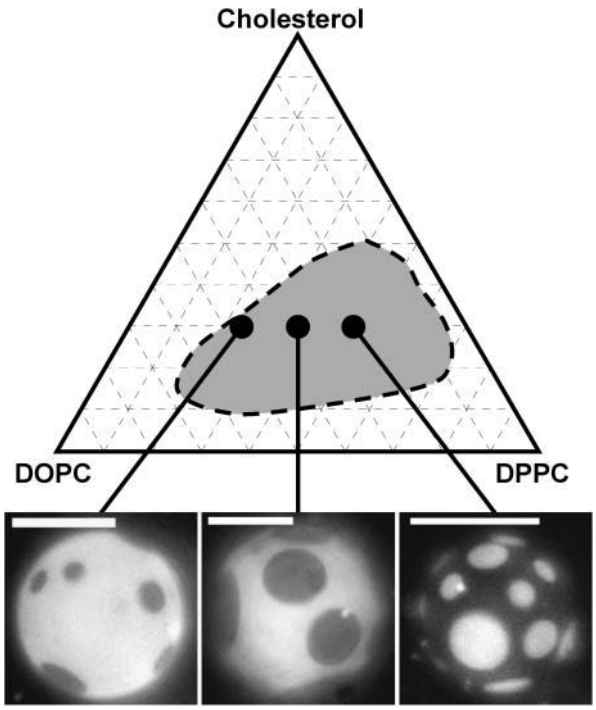

FIGURE 1 (*Top*) Sketch of miscibility phase boundary for ternary membranes of DOPC, DPPC, and cholesterol at 25°C (Veatch and Keller, 2003b). (*Bottom*) Fluorescence micrographs of GUVs with membrane composition studied by NMR. Vesicles are imaged at 25°C and compositions are 30% cholesterol mixed with (*from left to right*) 2:1 DOPC/DPPC, 1:1 DOPC/DPPC, and 1:2 DOPC/DPPC. Scale bars are 20 μm.

^{2}H-NMR

High temperature spectra of DPPC-d62 and Chol-d1

Throughout this section we will illustrate our points with the spectra in Fig. 2 for the mixture 1:1 DOPC/DPPC + 30% cholesterol. Complete DPPC-d62 spectra for all mixtures are in Fig. 3.

Above the miscibility transition temperature, vesicles are in a uniform L_α phase. Membranes labeled with Chol-d1 produce spectra with a single quadrupole splitting as at the top of Fig. 2 *A*. The signal is weak because the splitting is wide, and the molecule is labeled at only one location.

In contrast, ^{2}H-NMR spectra from membranes labeled with DPPC-d62 are a superposition of many quadrupole splittings since both acyl chains are fully deuterated. Wide splittings are due to ordered chain segments near the lipid water interface, and narrow splittings are due to more disordered segments near the bilayer center. The terminal methyl groups produce the smallest and most prominent splitting, shown at the top of Fig. 2 *C*. From the high temperature spectra, both Chol-d1 and DPPC-d62 are well mixed in the membrane and encounter roughly the same environment averaged over the ^{2}H-NMR timescale of 10 μs.

DPPC-d62 spectra at the miscibility transition

Demixing is observed as a loss of resolution in DPPC-d62 spectra as temperature is lowered through the miscibility transition. This is most evident in the methylene splittings of the shoulder of the spectra shown in the middle of Fig. 2 *B*. At temperatures between T_{mix} and T_{low} ^{2}H-NMR methylene resonances are poorly resolved, indicating that lipids exchange at rates of the order of $k \approx \pi\Delta\nu_q$. The largest difference in quadrupole splittings of methylene resonances between L_o and L_α domains is $\Delta\nu_q = 17$ kHz, corresponding to a domain size of ~80 nm.

We know of no obvious equilibrium mechanism that would reduce domain size to 80 nm in the MLVs used in our NMR studies from the micron-scale domains in the GUVs used in our fluorescence studies. Bilayers in MLVs are separated by a water layer of 1–2 nm (Petrache et al., 1998; Simon et al., 1995). Coupling between lamellae may contribute to domain size, although liquid domains of ~1 μm have been observed in supported membranes on a water layer of ~1 nm (Stottrup et al., 2004; van Duyl et al., 2003). We could also imagine, but have no evidence for, effects due to domain curvature, or coupling between lamellae of

TABLE 1 Miscibility transition temperatures (T_{mix}) and lower transition temperatures (T_{low}) for membranes of DPPC, DOPC, and cholesterol using different methods

	T_{mix}			T_{low}	
	Microscopy	^{2}H-NMR	^{1}H-MAS NMR	Microscopy	^{2}H-NMR
2:1 DOPC/DPPC-d62 + 30% Chol	24 ± 1°C	24 ± 2°C		12 ± 2°C	12 ± 2°C
2:1 DOPC/DPPC + 30% Chol-d1	29 ± 1°C				15 ± 5°C
2:1 DOPC/DPPC + 30% Chol	29 ± 1°C				
1:1 DOPC/DPPC-d62 + 30% Chol	29 ± 1°C	29 ± 1°C		21 ± 2°C	21 ± 1°C
1:1 DOPC/DPPC + 30% Chol-d1	32 ± 1°C				26 ± 1°C
1:1 DOPC/DPPC + 30% Chol	32 ± 1°C		32 ± 1°C	21 ± 3°C	
1:2 DOPC/DPPC-d62 + 30% Chol	33 ± 1°C	33 ± 1°C		28 ± 3°C	29 ± 1°C
1:2 DOPC/DPPC + 30% Chol-d1	36 ± 1°C				>30°C
1:2 DOPC/DPPC + 30% Chol	36 ± 1°C				

^{2}H-NMR experiments used deuterated lipid samples (either DPPC-d62 or Chol-d1), ^{1}H-MAS NMR measurements used only protonated lipids, and fluorescent microscopy measurements were conducted on both protonated and deuterated lipid mixtures. In microscopy experiments, T_{mix} marks the onset of μm-scale demixing in GUVs. In ^{1}H-MAS NMR experiments, significant spectral broadening initiates at T_{mix} and using ^{2}H-NMR, a plateau begins in the first moment of DPPC-d62 spectra. In ^{2}H-NMR, superposition of L_o and L_α phases are first observed at T_{low}. Additional evidence for a transition at T_{low} is seen as saturation in the surface fraction of dark phase in microscopy experiments.

domains with different bilayer thicknesses (Gandhavadi et al., 2002; Rinia et al., 2001).

The DPPC-d62 spectra provide additional evidence for a miscibility transition by examining the first moment, which is a measure of the average splitting and the overall order of the lipid chain. Fig. 4 shows the first moment as a function of temperature for the three mixtures studied. At the highest temperature, the first moment is lowest and the lipid chains are the most disordered. Decreasing temperature causes an increase in chain order, as is expected for lipids in a liquid phase. At the miscibility transition temperature, the value of the first moment reaches a plateau (*open symbols* in Fig. 4). This plateau continues with decreasing temperature until large (≫160 nm) domains are observed by ^{2}H-NMR (see next section). This trend is most clearly seen in the mixture of 1:1 DOPC/DPPC-d62 + 30% cholesterol, which has several data points in the plateau region.

Low temperature domains of ≫160 nm

A dramatic change is observed in both Chol-d1 and DPPC-d62 spectra at a temperature below the miscibility transition. At this point, which we call T_{low}, the number of splittings in ^{2}H-NMR spectra increases (Figs. 2 and 3). At temperatures below T_{low} resonances are a superposition of spectra from L_o and L_α domains. Therefore, at these temperatures, $k \ll \pi\Delta\nu_q$. Even the small difference in quadrupole splittings of terminal methyl resonances, $\Delta\nu_q = 3.8$ kHz, is well resolved, corresponding to a domain size of $d_o \gg 160$ nm.

The bottom of Fig. 2 shows low temperature spectra for membranes labeled with Chol-d1 and DPPC-d62. For Chol-d1, two peaks are observed, suggesting that two types of liquid environments are present in which the average orientation of cholesterol differs. Wider splittings result from more ordered lipids. For this mixture, the integrated intensity of the outer peak is larger, indicating that most of

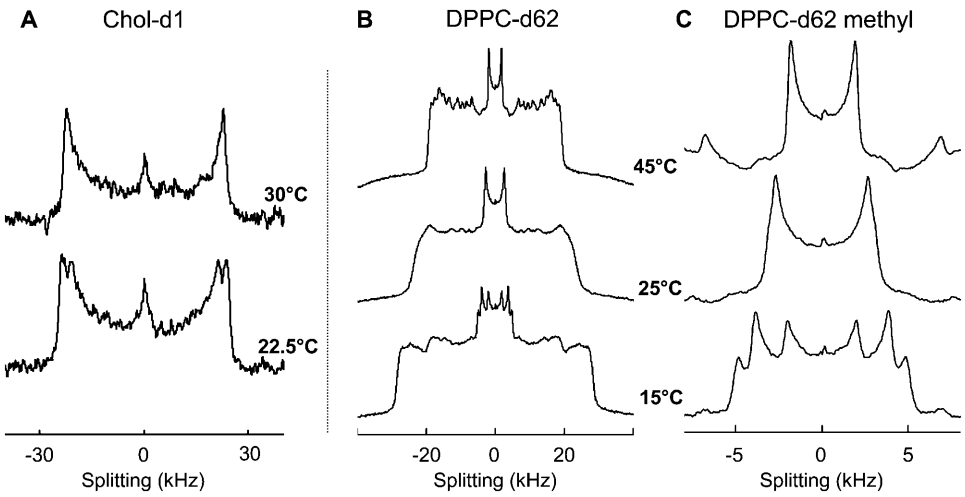

FIGURE 2 Selected ^{2}H-NMR spectra for MLVs of (*A*) 1:1 DOPC/DPPC + 30% Chol-d1 and (*B*,*C*) 1:1 DOPC/DPPC-d62 + 30% Chol. Spectra in *C* are an expanded view of the terminal methyl splitting in *B*. At low temperature (22.5°C in *A* and 15°C in *B*,*C*), multiple splittings are present in both Chol-d1 and in the methyl region of DPPC-d62 indicating that large-scale (≫160 nm) phase separation has occurred.

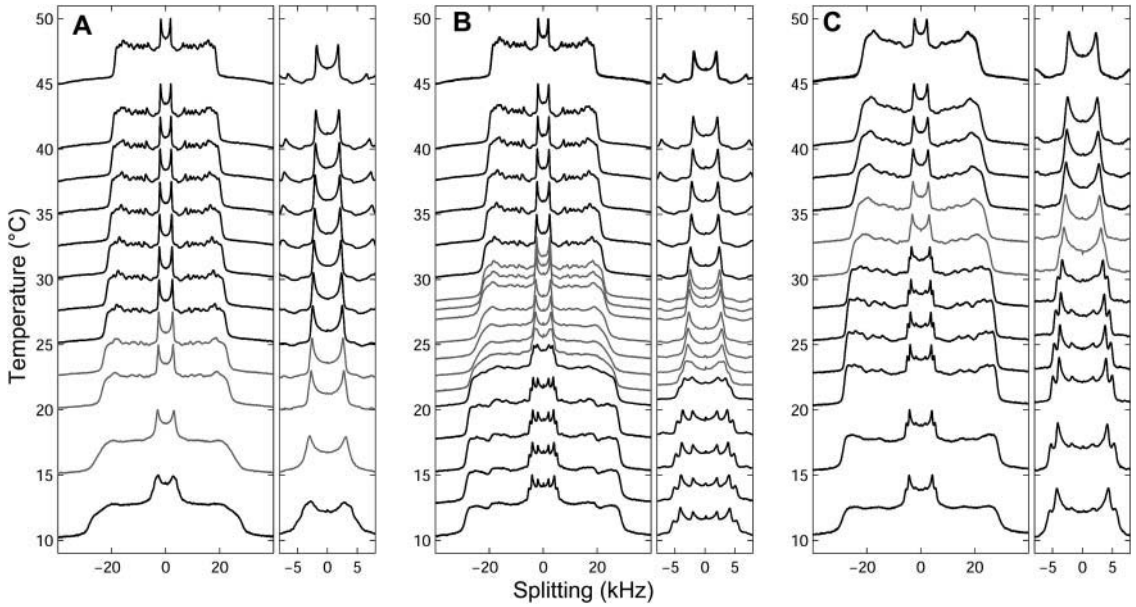

FIGURE 3 Temperature stack of ^{2}H-NMR spectra from MLVs of (*A*) 2:1 DOPC/DPPC-d62 + 30% Chol, (*B*) 1:1 DOPC/DPPC-d62 + 30% Chol, and (*C*) 1:2 DOPC/DPPC-d62 + 30% Chol. Spectra in shaded gray show reduced resolution and are obtained between T_{mix} and T_{low}.

the Chol-d1 is in the more ordered phase. Lipid compositions will be quantified in the section below titled Characterizing Liquid Phases by ^{2}H-NMR. DPPC-d62 behaves similarly, but the peak from the methyl group splits into three peaks. The inner peak is due to DPPC-d62 in the less ordered L_α phase. The two outer peaks stem from nonequivalence of the terminal methyl groups of the *sn*-1 and *sn*-2 chains of DPPC-d62 in a liquid-ordered state (Vist and Davis, 1990). These two peaks have equal intensity, independent of membrane temperature and composition, providing evidence that they arise from the same phase. The summed outer peaks have a larger intensity than the inner peak, indicating most of the DPPC-d62 is in the L_o phase. The two distinct wide and broad unresolved peaks in the shoulder of the spectrum at the bottom of Fig. 2 *B* are from the remaining deuterated groups, and are further evidence for the superposition of two (and only two) spectra.

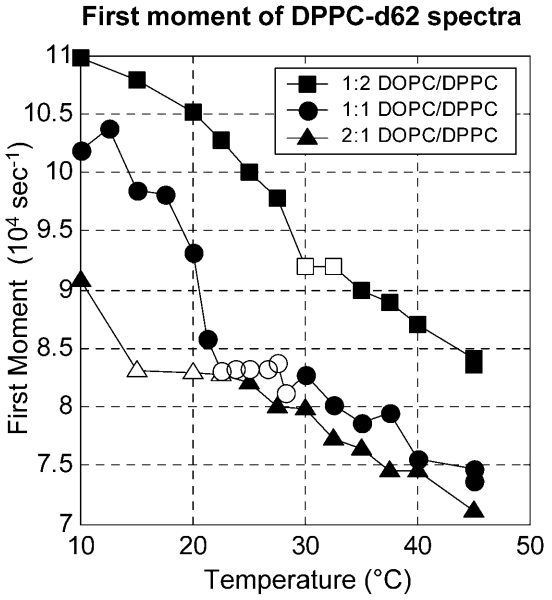

FIGURE 4 First moment of DPPC-d62 spectra in ■□ 1:2 DOPC/DPPC-d62 + 30% Chol, ●○ 1:1 DOPC/DPPC-d62 + 30% Chol, and ▲△ 2:1 DOPC/DPPC-d62 + 30% Chol membranes. Open symbols depict the plateau region between T_{low} and T_{mix}. ●○ points were obtained by both decreasing and increasing temperature.

The same low temperature event is evident in the first moment of DPPC-d62 spectra. As temperature decreases, there is an increase in the first moment at the same temperature where multiple methyl peaks first appear in DPPC-d62 spectra. This may indicate either a simple change in domain size or a significant ordering transition. Below T_{low}, the first moment again increases with decreasing temperature, as expected for lipids in a liquid state. The transition temperatures, T_{low} and T_{mix}, derived from ^{2}H-NMR experiments, are compiled in Table 1.

In summary, ^{2}H-NMR of MLVs finds three distinct regions. At high temperatures, both DPPC-d62 and Chol-d1 spectra indicate that membranes are in a uniform L_α phase. At the miscibility transition temperature, the DPPC-d62 spectra lose resolution and the first moment enters a plateau region. This suggests exchange of lipids between environments on the ^{2}H-NMR timescale and small domains ($\sim$80 nm). At low temperatures, large-scale ($\gg$160 nm) demixing into a L_α and L_o phase is observed for all lipid mixtures studied.

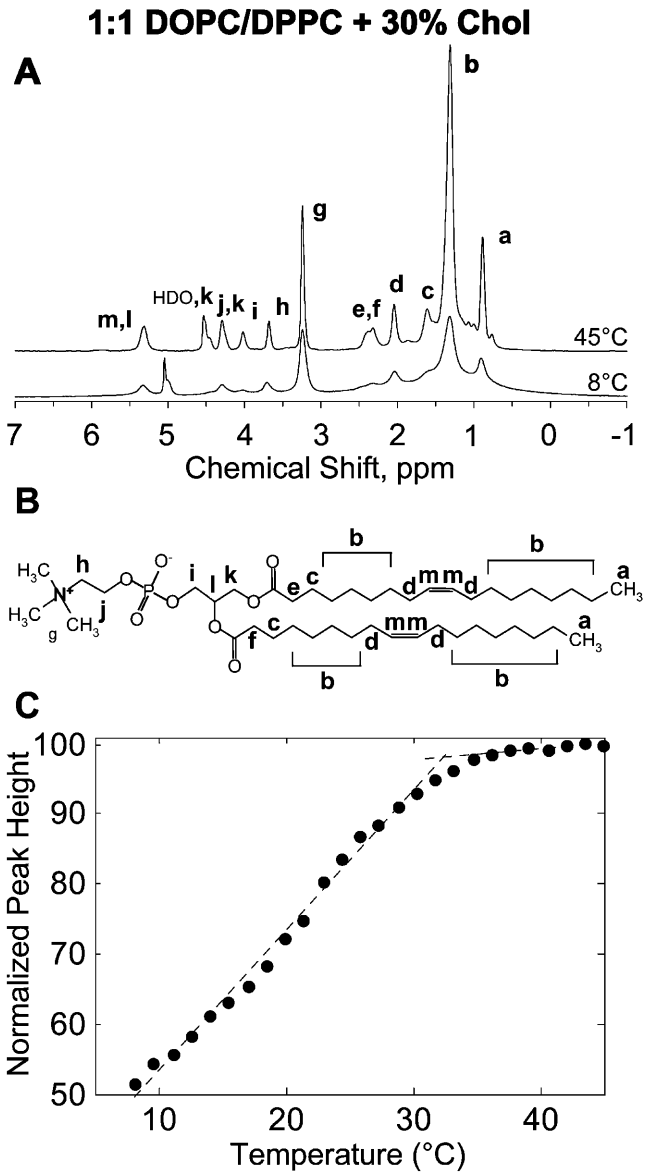

FIGURE 5 (*A*) Proton magic angle spinning NMR spectra of multilamellar vesicles of 1:1 DOPC:DPPC + 30% cholesterol. The top spectrum was acquired at 45°C and the bottom at 8°C. (*B*) Assignment of major lipid resonances is illustrated using molecular structure of DOPC. DPPC has essentially the same spectrum but lacks signals related to the double bond (*d*, *m*) and has a different number of saturated methylenes (*b*). (*C*) Peak height of the methylene proton resonance at 1.3 ppm normalized to the signal at 45°C. Lower peak heights at lower temperatures indicate a larger fraction of ordered component. The onset of demixing at T_{mix} agrees with fluorescent microscopy results. Error bars are smaller than data points, suggesting that the small change in slope near 20°C may be evidence of a transition at T_{low}.

^{1}H-MAS NMR

Further evidence for coexisting L_α and L_o phases at temperatures lower than T_{mix} was obtained by ^{1}H-MAS NMR for 1:1 DOPC/DPPC mixed with 30% cholesterol. Resonances of the L_o phase are substantially broadened compared to the more fluid L_α phase when spectra are acquired as described in Materials and Methods. The difference in peak width between phases is particularly large for the strong resonance of chain methylene protons at 1.3 ppm (Fig. 5 *A*). Results are reported as peak height, which is inversely related to peak width and can be determined with minimal error in a model-independent manner (Fig. 5 *C*).

In experiments on binary DPPC/cholesterol and SOPC/cholesterol mixtures we have established that the broadening of resonances in the liquid-ordered and solid-ordered states is the result of an increase in the effective strength of proton dipole-dipole interactions between neighboring methylene groups (I. V. Polozov and K. Gawrisch, unpublished data). The stronger dipole interactions result in homogenous broadening of resonances that is not averaged out by MAS. This analysis measures spectral broadening, not signal superposition, and is sensitive to formation of liquid-ordered domains of any size. Formation of large domains lowers peak height by superposition of broad L_o and narrow L_α resonances.

Fig. 5 *C* shows the height of the methylene resonance peak as a function of temperature, normalized to the high temperature signal. We observe a decrease in peak height with decreasing temperature reflecting an increase in the amount of L_o phase in the membrane. Although contributions from temperature-dependent broadening in the L_α phase have been suppressed (see Materials and Methods), additional spectral broadening may arise from increased order of lipids in the L_o phase at low temperatures.

The plot in Fig. 5 *C* can be approximated by two linear functions that intersect at the onset of L_o/L_α phase coexistence (32 ± 1°C). This is in excellent agreement with the corresponding transition detected by fluorescence microscopy on protonated lipids shown in Table 1.

Fluorescence microscopy of deuterated membranes

In our previous work, we used fluorescence microscopy to identify a miscibility transition at T_{mix}. The NMR results above identify two different transitions, at T_{mix} and T_{low}. In this section, we present additional fluorescence microscopy evidence for a transition at T_{low}.

Below the miscibility transition, fluorescence microscopy shows two phases, one bright and one dark, in GUVs of DOPC, DPPC, and cholesterol. Qualitatively, the dark phase is more ordered and is enriched in cholesterol and DPPC. Fig. 6 shows the surface fraction of dark phase as a function of temperature in GUVs of three mixtures studied. At high temperature, vesicles are in one uniform phase at the μm-scale and no dark phase is present. Lowering temperature, vesicles phase-separate at the miscibility transition. The temperatures T_{mix} and T_{low} are denoted by dashed lines in Fig. 6. Between these temperatures, the surface fraction of dark phase is smallest and increases as temperature is lowered. There is no evidence for small (<1 μm) length-

scale lipid organization by fluorescence microscopy in this temperature regime. Below $\sim T_{low}$, the surface fraction of dark phase saturates and is roughly constant. This is most clearly seen in membranes of 1:1 DOPC/DPPC-d62 + 30% cholesterol because each temperature range is well represented in Fig. 6 *B*.

Characterizing liquid phases by ^{2}H-NMR

As discussed above in the ^{2}H-NMR section, near the miscibility transition temperature, domains observed by NMR in MLVs are smaller than by fluorescence microscopy in GUVs. It has not escaped our attention that there may be an offset in the transition temperature in the two systems. Nevertheless, we believe our data is best described by a difference in domain size rather than transition temperature. This assertion is based on the following evidence: 1), Both ^{2}H-NMR and ^{1}H-MAS NMR observe the onset of demixing into ordered and disordered phases, at the miscibility transition. 2), Both ^{2}H-NMR and fluorescent microscopy detect a second transition at lower temperature. In this section, we use our low temperature ^{2}H-NMR spectra to analyze trends in lipid order within coexisting phases, to quantify the fraction of cholesterol and DPPC in these phases, and to construct tie-lines in the DOPC/DPPC/cholesterol ternary phase diagram.

Trends in lipid order

For cholesterol, the magnitude of the quadrupole splitting reflects movement of the 3α C-^{2}H bond with respect to the bilayer normal. Assuming the average cholesterol orientation does not change, then differences between quadrupole splittings are entirely due to differences of the cone angle through which cholesterol wobbles in the two phases (see Materials and Methods). Fig. 7, *A–C* shows the Chol-d1 splittings and associated wobble angles as a function of temperature. The wobble angle in L_o domains generally decreases with decreasing temperature, reflecting an expected increase in order.

The results are similar for membranes labeled with DPPC-d62 as shown in Fig. 7, *D–F*. Below T_{low}, DPPC-d62 spectra show three terminal methyl peaks, two from the L_o phase and one from the more disordered L_α phase. As temperature is lowered, the width of the two wide splittings in the L_o phase increase, indicating that order increases in that phase. In contrast, the methyl splittings from DPPC-d62 in the L_α phase decrease with decreasing temperature, indicating more disorder. The quantity of DPPC-d62 in the L_α phase also decreases (see next section) and should explain this behavior.

Partitioning of DPPC and cholesterol

Fig. 8 quantifies how DPPC-d62 and Chol-d1 are distributed between the two coexisting liquid phases. Spectra were fit as described in the Materials and Methods section. Fig. 8 *A* demonstrates that DPPC strongly partitions into the L_o phase. A majority of the DPPC present in the membrane is found in the ordered phase at all compositions and temperatures studied. In general, there is a trend of increasing DPPC fraction in the ordered phase as the DOPC/DPPC fraction changes from 2:1 to 1:2. This trend is repeated in cholesterol,

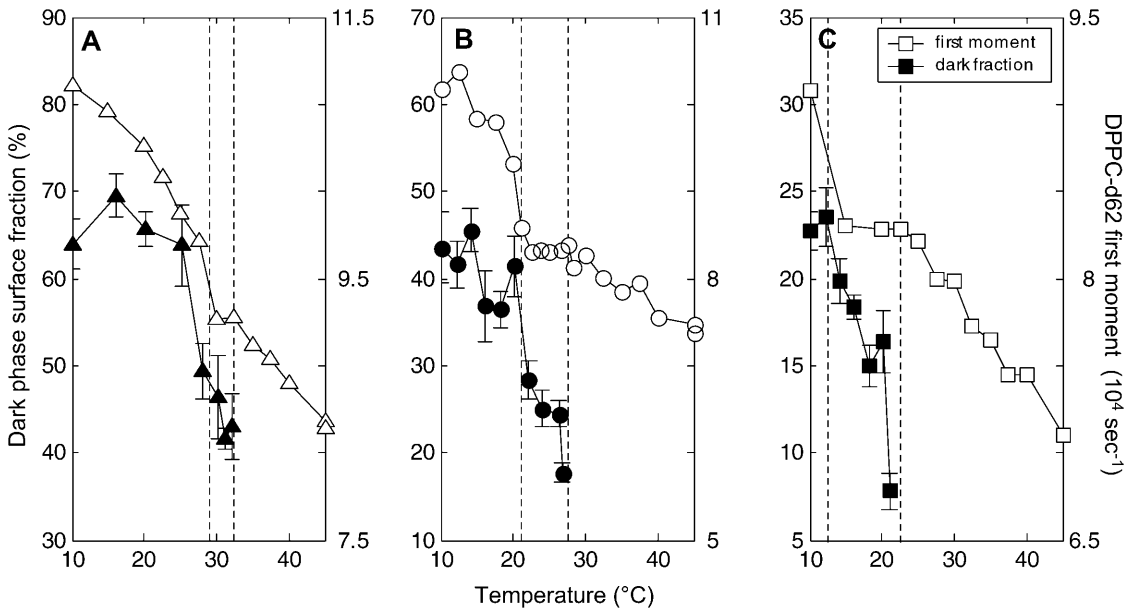

FIGURE 6 First moment of DPPC-d62 spectra (*open symbols*) and surface fraction of dark phase from fluorescence micrographs (*solid symbols*) for membranes of ■□ 1:2 DOPC/DPPC-d62+30% Chol, ●○ 1:1 DOPC/DPPC-d62+30% Chol, and ▲△ 2:1 DOPC/DPPC-d62 + 30% Chol.

from which we conclude that cholesterol is associated with DPPC in an ordered phase. Unlike DPPC, Chol-d1 partitions less strongly into the L_o phase. In membranes of 2:1 DOPC/DPPC + 30% Chol-d1, the majority of Chol-d1 is in the more disordered L_α phase. This does not necessarily imply a lower cholesterol concentration is present in the L_o phase than in the L_α phase. Instead, it is likely that there is very little of the L_o phase in these membranes. This is consistent with the fluorescence micrograph in the bottom left of Fig. 1 in which little of the dark, ordered, DPPC-rich phase is present. The quantitative conclusions in Fig. 8 mirror our previous qualitative observations using fluorescence microscopy (Veatch and Keller, 2003b).

Tie-lines in the DOPC/DPPC/cholesterol miscibility phase diagram

Using our NMR data and our previously determined miscibility phase diagram, we estimate several tie-lines within the liquid coexistence region. The two compositions shown are 30% cholesterol mixed with either 1:1 DOPC/DPPC at 25°C (Fig. 9 *A*), or with 1:2 DOPC/DPPC at multiple temperatures (Fig. 9 *B*). The overall conclusion from Fig. 9 *B* is that the cholesterol compositions of the ordered and disordered phases become more equal when temperature decreases. Nearly equal cholesterol compositions result in nearly horizontal tie-lines. Tie-lines are also more horizontal when more DPPC is present in the membrane (Fig. 9 *C*).

Unfortunately, we are unable to draw specific conclusions regarding area per molecule of lipids in the coexisting phases due to large errors in surface fraction measurements. Nevertheless, surface fraction and tie-line results are consistent with a lipid density in the L_o phase being less than factor of two greater than the lipid density present in the L_α phase ($\rho_o/\rho_\alpha < 2$). This limiting case is consistent with recent simulation results that the average area per molecule in 2:1 mixtures of DPPC and cholesterol is roughly 40 Å^2 (Chiu et al., 2002). This composition resembles the L_o phase and the quoted area per molecule is averaged over both DPPC and cholesterol moieties. The primary component of the L_α phase, DOPC, occupies a significantly larger area, ~70 Å^2 (Nagle and Tristram-Nagle, 2000). This evidence suggests that the ratio of densities between the L_o and L_α phases is $\rho_o/\rho_\alpha < 1.8$.

Based on the calculated tie-lines, we can evaluate the apparent free energy of transfer between phases (ΔG) for each component. In Table 2, we present values for $\Delta G = -k_B T \ln(K)$, where k_B is the Boltzmann factor, T is the temperature, and K is either the mole fraction partition coefficient (i.e.,

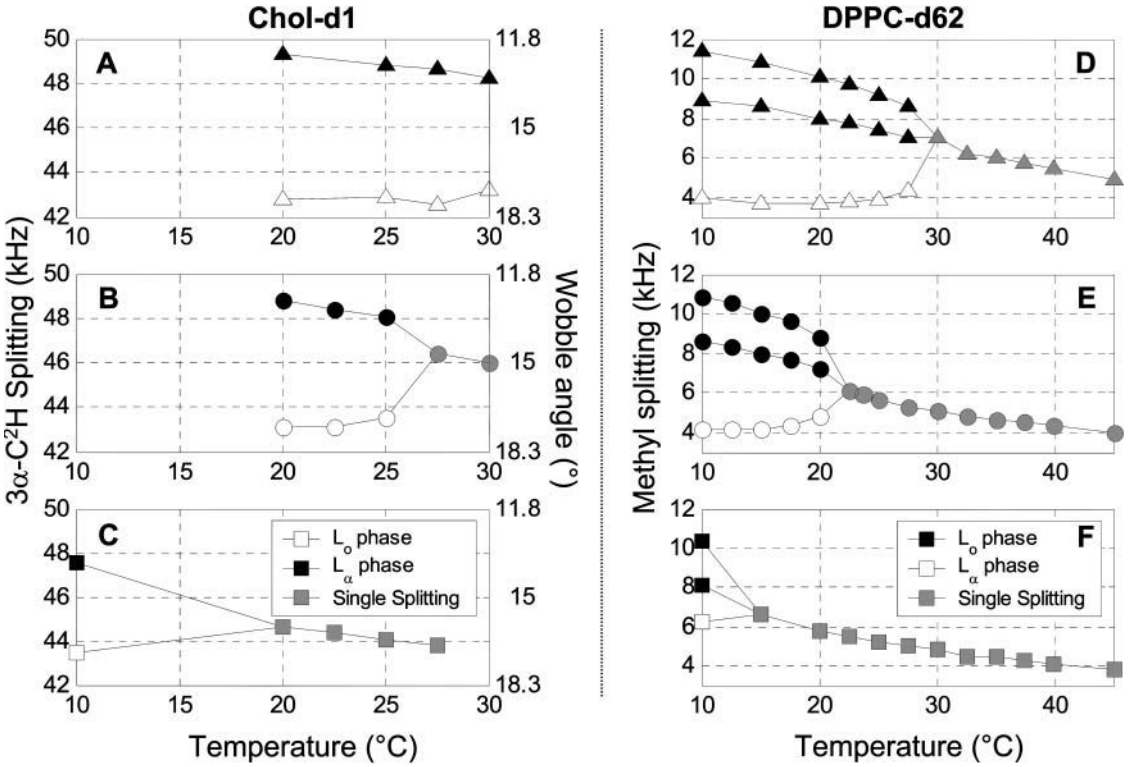

FIGURE 7 (*A–C*) Magnitude of 3α C-^{2}H splitting in Chol-d1 spectra (*left axis*) and associated wobble angle (*right axis*) in membranes of (*A*) 1:2 DOPC/DPPC + 30% Chol-d1, (*B*) 1:1 DOPC/DPPC + 30% Chol-d1, and (*C*) 2:1 DOPC/DPPC + 30% Chol-d1. White (*black*) symbols label the L_α (L_o) phase when multiple peaks are present. (*D–F*) Magnitude of DPPC-d62 terminal methyl splitting in membranes of (*D*) 1:2 DOPC/DPPC-d62 + 30% Chol, (*E*) 1:1 DOPC/DPPC-d62 + 30% Chol, and (*F*) 2:1 DOPC/DPPC-d62 + 30% Chol. Again, white (*black*) symbols label the L_α (L_o) phase when multiple peaks are present. Two sets of L_o phase splittings are present at low temperature and are due to nonequivalence of the *sn*-1 and *sn*-2 methyl peaks in that phase (see text).

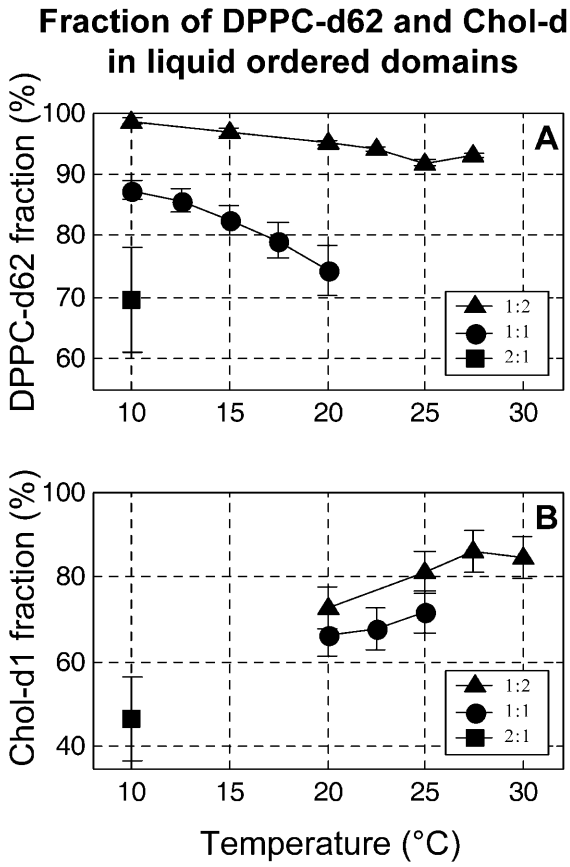

FIGURE 8 Fraction of (*A*) DPPC-d62 and (*B*) Chol-d1 in liquid-ordered domains (as opposed to L_α domains). Membranes are composed of 30% Chol (or Chol-d1) with either ■ 1:2 DOPC/DPPC (or DPPC-d62), ● 1:1 DOPC/DPPC (or DPPC-d62), or ▲ 2:1 DOPC/DPPC (or DPPC-d62).

$K_X^{DPPC} = X_o^{DPPC}/X_\alpha^{DPPC}$) or molar partition coefficient (i.e., $K_M^{DPPC} = [DPPC]_o/[DPPC]_\alpha$) (White and Wimley, 1999). Any differences between ΔG_X and ΔG_M arise from density differences between L_o and L_α phases. In all cases, DPPC partitions strongly into the L_o plase and DOPC into the L_α phase. In contrast, ΔG values for cholesterol are generally smaller than k_BT, suggesting that individual cholesterol molecules move between phases without a significant energy cost. These values are consistent with those measured in similar lipid mixtures using detergent resistance (McIntosh et al., 2003).

The tie-line calculation above depends on assumptions, which are listed here and in Materials and Methods for completeness. First, we assume that the fluorescent-microscopy derived miscibility phase diagram can be used in concert with ^{2}H-NMR results. This assumption appears valid because even though domain sizes differ between NMR and microscopy experiments, both methods detect demixing in membranes at the miscibility transition temperature. Additionally, we assume that the substitution of DPPC-d62 for DPPC lowers the transition temperature by a constant offset of ~2.5°C. The offset is larger for membranes of 2:1 DOPC/DPPC + 30% cholesterol (Table 1), and will contribute to errors in the tie-lines. Errors also arise due to uncertainties in the miscibility phase diagram itself, which are documented in Veatch and Keller (2003b).

COMPARISON TO RECENT LITERATURE

The experiments above present a framework for interpreting other ^{2}H-NMR results published in the past year. Van Duyl et al. (2003) studied MLVs of equimolar DOPC, cholesterol, and either egg sphingomyelin (SM) or DPPC. Membranes containing egg SM, DOPC, and cholesterol undergo a reordering transition between 40 and 50°C. This range is consistent with the miscibility transition of 42 ± 2°C that we observe by fluorescence microscopy (Veatch and Keller, 2003b). They too do not report superposition of peaks below this transition indicating that domains are small (~80 nm). We suspect that large-scale (≫160 nm) demixing occurs in these membranes at a lower temperature, which was not

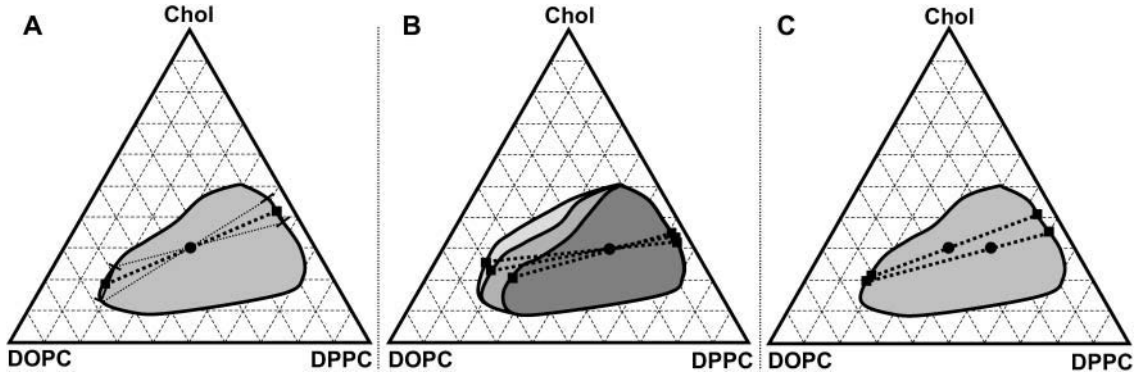

FIGURE 9 Estimated tie-lines in DOPC/DPPC/cholesterol ternary phase diagram. (*A*) The tie-line for the mixture of 1:1 DOPC/DPPC + 30% cholesterol at 25°C is denoted by a thick dashed line. Thin dashed lines are bounds on the errors and are representative of all calculated tie-lines. (*B*) Phase boundary and tie-lines for 1:2 DOPC/DPPC + 30% cholesterol membranes at 30°C (*dark shaded*), 25°C (*medium shaded*), and 20°C (*light shaded*). (*C*) Tie-lines through the points 1:1 and 1:2 DOPC/DPPC + 30% cholesterol at 25°C.

TABLE 2 Phase compositions and apparent free energy of transfer between L_o and L_α phases (ΔG) for mixtures with estimated tie-lines

	Temp	Lipid	X_0	X_α	ΔG_X	$\Delta G_X/k_BT$	$\Delta G_M/k_BT$
1:2 DOPC/DPPC + 30% Chol	20°C	DOPC	05 ± 2%	60 ± 3%	+1.4 ± 0.26	+2.5 ± 0.45	+1.8 to +2.5
		DPPC	63 ± 2%	13 ± 3%	−0.92 ± 0.15	−1.6 ± 0.26	−2.3 to −1.6
		Chol	32 ± 2%	27 ± 3%	−0.10 ± 0.10	−0.17 ± 0.17	−0.86 to −0.17
	25°C	DOPC	05 ± 2%	59 ± 3%	+1.5 ± 0.27	+2.5 ± 0.45	+1.8 to +2.5
		DPPC	61 ± 2%	18 ± 3%	−0.72 ± 0.12	−1.2 ± 0.20	−1.9 to −1.2
		Chol	34 ± 2%	23 ± 3%	−0.23 ± 0.11	−0.39 ± 0.19	−1.1 to −0.39
	30°C	DOPC	05 ± 2%	55 ± 3%	+1.4 ± 0.27	+2.4 ± 0.45	+1.7 to +2.4
		DPPC	59 ± 2%	25 ± 3%	−0.52 ± 0.09	−0.86 ± 0.15	−1.5 to −0.86
		Chol	36 ± 2%	20 ± 3%	−0.35 ± 0.12	−0.59 ± 0.21	−1.3 to −0.59
1:1 DOPC/DPPC + 30% Chol	20°C	DOPC	05 ± 2%	59 ± 3%	+1.4 ± 0.26	+2.5 ± 0.45	+1.8 to +2.5
		DPPC	53 ± 2%	14 ± 3%	−0.77 ± 0.15	−1.3 ± 0.25	−2.0 to −1.3
		Chol	42 ± 2%	27 ± 3%	−0.26 ± 0.09	−0.44 ± 0.16	−1.1 to −0.44
	25°C	DOPC	05 ± 2%	60 ± 3%	+1.5 ± 0.27	+2.5 ± 0.45	+1.8 to +2.5
		DPPC	53 ± 2%	18 ± 3%	−0.63 ± 0.12	−1.1 ± 0.20	−1.8 to −1.1
		Chol	32 ± 2%	22 ± 3%	−0.38 ± 0.11	−0.65 ± 0.18	−1.3 to −0.65
1:2 DOPC/DPPC + 30% Chol	10°C	DOPC	05 ± 2%	58 ± 3%	+1.4 ± 0.25	+2.5 ± 0.45	+1.8 to +2.5
		DPPC	32 ± 2%	13 ± 3%	−0.50 ± 0.16	−0.90 ± 0.29	−1.6 to −0.90
		Chol	43 ± 2%	29 ± 3%	−0.22 ± 0.08	−0.39 ± 0.15	−1.1 to −0.39

The X_o and X_α columns show the composition (mol %) of each component in coexisting L_o and L_α phases. ΔG_X and ΔG_M are evaluated from mol fraction (X) and molar (M) free energy basis states (White and Wimley, 1999). Units for ΔG_X are kcal/mol. Errors are estimated from tie-line and phase boundary uncertainties. ΔG_M is presented as a range of possible values (ΔG_X–k_BT ln(2) to ΔG_X) due to the large uncertainty in density differences between phases ($1 < \rho_o/\rho_\alpha < 2$).

probed. These researchers also studied membranes containing DPPC, but temperatures below the fluorescence miscibility transition of 29 ± 1°C were not probed and, consequently, reorganization of DOPC was not observed.

A separate research group (Aussenac et al., 2003) conducted ^{2}H-NMR measurements on equimolar mixtures of POPC, porcine brain SM, and cholesterol. Unfortunately, at the temperatures chosen, no liquid domains are observed in GUVs of this lipid mixture by fluorescence microscopy (Veatch and Keller, 2003b). As we would predict, the authors found no overlap of powder spectra in the same temperature range.

We are not fully comfortable describing ~80 nm domains in MLVs between T_{low} and T_{mix} as coexisting liquid phases. On one hand, a bilayer domain of 80 nm diameter could contain over 15,000 lipids. On the other hand, we have previously emphasized that nanoscale organization does not necessarily indicate the coexistence of two separate phases. Instead, it may describe complex intermolecular interactions occurring within a single phase (Veatch and Keller, 2003b). GUVs of lipid mixtures described in this manuscript exhibit macroscopic separation into coexisting phases below the miscibility transition by fluorescence microscopy. Using NMR, it is less clear how to classify the true phase boundary in MLVs. We present evidence for demixing by NMR at the miscibility transition temperature, but large-scale ($\gg$160 nm) domains are not observed until lower temperatures. One option is that the GUV miscibility phase boundary is simply shifted to lower temperatures in MLVs. We do not believe this is the case. Coupling between adjacent lamellae should instead stabilize coexisting phases and raise the miscibility transition temperature. Others have suggested that the fluorescent probes affect transition temperatures (Aussenac et al., 2003). We found no dependence on miscibility transition temperature when probe concentration varied from 0.2% to 2%. We conclude that MLVs observed by NMR do undergo phase separation at the miscibility transition, but either the geometry of the membrane limits domain size or the character of the coexisting phases gives the impression of small domains.

These questions of domain size and transition temperature in ternary mixtures of saturated lipids, unsaturated lipids, and cholesterol are further complicated by recent experiments using fluorescence resonance energy transfer. Several groups have found that domains of >10 nm persist in MLV membranes to temperatures well above the miscibility transition (de Almeida et al., 2003; Silvius, 2003). These results reemphasize the complexity present in these simple membranes.

CONCLUSION

We show that ^{2}H-NMR, ^{1}H-MAS NMR, and fluorescence microscopy detect liquid demixing at the miscibility transition temperature, T_{mix}, in three separate mixtures of DOPC, DPPC, and cholesterol. Slightly below the miscibility transition temperature, NMR experiments on MLVs detect domains with diameters ~80 nm whereas microscopy experiments in GUVs observe >1 μm domains. At a lower

temperature, T_{low}, ^{2}H-NMR spectra reveal large-scale demixing into $\gg$160 nm domains of L_o and L_α phases. We quantitatively determine that the L_o phase is enriched in DPPC and cholesterol. Based on these observations and the previously published DPPC/DOPC/cholesterol miscibility phase diagram, we estimate tie-lines at different temperatures and membrane compositions. Our results are consistent with recent studies by other groups and provide a framework for interpreting ^{2}H-NMR measurements in similar membranes.

We thank Ben Stottrup, Walter Teague, Harden McConnell, Michael Schick, Kirill Katsov, and Richard Elliott.

S.L.V. was supported in part by a National Institutes of Health predoctoral training grant in molecular biophysics (5T32-GM08268-14) and a National Science Foundation fellowship from the UW Center for Nanotechnology. I.V.P. and K.G. are supported by the Intramural Research Program of National Institute on Alcohol Abuse and Alcoholism, National Institutes of Health. S.L.K. acknowledges support from a National Science Foundation Career Award MCB#0133484, from the Research Corporation (Research Innovation Award and Cottrell Scholar Award), and from the Petroleum Research Fund, administered by the American Chemical Society.

REFERENCES

Alecio, M. R., D. E. Golan, W. R. Veatch, and R. R. Rando. 1982. Use of a fluorescent cholesterol derivative to measure lateral mobility of cholesterol in membranes. *Proc. Natl. Acad. Sci. USA.* 79:5171–5174.

Anderson, R. G., and K. Jacobson. 2002. A role for lipid shells in targeting proteins to caveolae, rafts, and other lipid domains. *Science.* 296:1821–1825.

Angelova, M. I., S. Soleau, P. Meleard, J. F. Faucon, and P. Bothorel. 1992. Preparation of giant vesicles by external AC electric fields. Kinetics and applications. *Progr. Colloid Polym. Sci.* 89:127–131.

Aussenac, F., M. Tavares, and E. J. Dufourc. 2003. Cholesterol dynamics in membranes of raft composition: a molecular point of view from ^{2}H and ^{31}P solid-state NMR. *Biochemistry.* 42:1383–1390.

Baumgart, T., S. T. Hess, and W. W. Webb. 2003. Imaging coexisting fluid domains in biomembrane models coupling curvature and line tension. *Nature.* 425:821–824.

Brown, D. A., and E. London. 1998. Functions of lipid rafts in biological membranes. *Annu. Rev. Cell Dev. Biol.* 14:111–136.

Brzustowicz, M. R., V. Cherezov, M. Caffrey, W. Stillwell, and S. R. Wassall. 2002. Molecular organization of cholesterol in polyunsaturated membranes: microdomain formation. *Biophys. J.* 82:285–298.

Chiu, S. W., E. Jakobsson, R. J. Mashl, and H. L. Scott. 2002. Cholesterol-induced modifications in lipid bilayers: a simulation study. *Biophys. J.* 83:1842–1853.

Davis, J. H., K. R. Jeffrey, M. Bloom, M. I. Valic, and T. P. Higgs. 1976. Quadrupolar echo deuteron magnetic resonance spectroscopy in ordered hydrocarbon chains. *Chem. Phys. Lett.* 42:390–394.

de Almeida, R. F. M., A. Fedorov, and M. Prieto. 2003. Sphingomyelin/phosphatidylcholine/cholesterol phase diagram: boundaries and composition of lipid rafts. *Biophys. J.* 85:2406–2416.

Dietrich, C., L. A. Bagatolli, Z. N. Volovyk, N. L. Thompson, M. Levi, K. Jacobson, and L. A. Gratton. 2001. Lipid rafts reconstituted in model membranes. *Biophys. J.* 80:1417–1428.

Gaede, H. C., and K. Gawrisch. 2003. Lateral diffusion rates of lipid, water, and a hydrophobic drug in a multilamellar liposome. *Biophys. J.* 85: 1734–1740.

Gandhavadi, M., D. Allende, A. Vidal, S. A. Simon, and T. J. McIntosh. 2002. Structure, composition, and peptide binding properties of detergent soluble bilayers and detergent resistant rafts. *Biophys. J.* 82:1469–1482.

Gidwani, A., D. Holowka, and B. Baird. 2001. Fluorescence anisotropy measurements of lipid order in plasma membranes and lipid rafts from RBL-2H3 mast cells. *Biochemistry.* 40:12422–12429.

Huang, J., J. T. Buboltz, and G. W. Feigenson. 1999. Maximum solubility of cholesterol in phosphatidylcholine and phosphatidylethanolamine bilayers. *Biochim. Biophys. Acta.* 1417:89–100.

Huster, D., and K. K. G. Arnold. 1998. Influence of docosahexaenoic acid and cholesterol on lateral lipid organization in phospholipid mixtures. *Biochemistry.* 37:17299–17308.

Kenworthy, A. K., N. Petranova, and M. Edidin. 2000. High-resolution FRET microscopy of cholera toxin B-subunit and GPI-anchored proteins in cell plasma membranes. *Mol. Biol. Cell.* 11:1645–1655.

Lentz, B. R., D. A. Barrow, and M. Hoechli. 1980. Cholesterol-phosphatidylcholine interactions in multilamellar vesicles. *Biochemistry.* 19:1943–1954.

London, E., and D. Brown. 2000. Insolubility of lipids in Triton X-100: physical origin and relationship to sphingolipid/cholesterol membrane domains (rafts). *Biochim. Biophys. Acta.* 1508:182–195.

McCabe, M. A., and S. R. Wassall. 1995. Fast-Fourier-transform dePaking. *J. Mag. Res. B.* 106:80–82.

McIntosh, T. J., A. Vidal, and S. A. Simon. 2003. Sorting of lipids and transmembrane peptides between detergent-soluble bilayers and detergent-resistant rafts. *Biophys. J.* 85:1656–1666.

McMullen, T. P., and R. N. McElhaney. 1995. New aspects of the interaction of cholesterol with dipalmitoylphosphatidylcholine bilayers as revealed by high-sensitivity differential scanning calorimetry. *Biochim. Biophys. Acta.* 1234:90–98.

Nagle, J. F., and S. Tristram-Nagle. 2000. Structure of lipid bilayers. *Biochim. Biophys. Acta.* 1469:159–195.

Oldfield, E., M. Meadows, D. Rice, and R. Jacobs. 1978. Spectroscopic studies of specifically deuterium-labeled membrane systems. Nuclear magnetic resonance investigation of the effects of cholesterol in model systems. *Biochemistry.* 17:2727–2740.

Petrache, H. I., N. Gouliaev, S. Tristram-Nagle, R. Zhang, R. M. Suter, and J. F. Nagle. 1998. Interbilayer interactions from high-resolution x-ray scattering. *Phys. Rev. E.* 57:7014–7024.

Rinia, H. A., M. Snel, J. van der Eerden, and B. de Kruijff. 2001. Visualizing detergent resistant domains in model membranes with atomic force microscopy. *FEBS Lett.* 501:92–96.

Samsonov, A. V., I. Mihalyov, and F. S. Cohen. 2001. Characterization of cholesterol-sphingomyelin domains and their dynamics in bilayer membranes. *Biophys. J.* 81:1486–1500.

Shimshick, E. J., and H. M. McConnell. 1973. Lateral phase separations in binary mixtures of cholesterol and phospholipids. *Biochem. Biophys. Res. Commun.* 53:446–451.

Silvius, J. R. 2003. Fluorescence energy transfer reveals microdomain formation at physiological temperatures in lipid mixtures modeling the outer leaflet of the plasma membrane. *Biophys. J.* 85:1034–1045.

Simon, S. A., S. Advani, and T. J. McIntosh. 1995. Temperature dependence of the repulsive pressure between phosphatidylcholine bilayers. *Biophys. J.* 69:1473–1483.

Simons, K., and E. Ikonen. 1997. Functional rafts in cell membranes. *Nature.* 387:569–572.

Sternin, E., M. Bloom, and A. L. MacKay. 1983. De-Paking of NMR spectra. *J. Mag. Res.* 55:274–282.

Stottrup, B. L., S. L. Veatch, and S. L. Keller. 2004. Nonequilibrium behavior in supported lipid membranes containing cholesterol. *Biophys. J.* 86:2942–2950.

Taylor, M. G., T. Akiyama, and I. C. Smith. 1981. The molecular dynamics of cholesterol in bilayer membranes: a deuterium NMR study. *Chem. Phys. Lipids.* 29:327–339.

van Duyl, B. Y., D. Ganchev, V. Chupin, B. de Kruijff, and J. A. Killian. 2003. Sphingomyelin is much more effective than saturated phosphatidylcholine in excluding unsaturated phosphatidylcholine from domains formed with cholesterol. *FEBS Lett.* 547:101–106.

Veatch, S. L., and S. L. Keller. 2002. Lateral organization in lipid membranes containing cholesterol. *Phys. Rev. Lett.* 89:268101.

Veatch, S. L., and S. L. Keller. 2003a. A closer look at the canonical ''raft mixture'' in model membrane studies. *Biophys. J.* 84:725–726.

Veatch, S. L., and S. L. Keller. 2003b. Separation of liquid phases in giant vesicles of ternary mixtures of phospholipids and cholesterol. *Biophys. J.* 85:3074–3083.

Vist, M. R., and J. H. Davis. 1990. Phase equilibria of cholesterol/dipalmitoylphosphatidylcholine mixtures: ^{2}H nuclear magnetic resonance and differential scanning calorimetry. *Biochemistry.* 29:451–464.

White, S. H., and W. C. Wimley. 1999. Membrane protein folding and stability. Physical principles. *Annu. Rev. Biophys. Biomol. Struct.* 28:319–365.